DOI: 10.1002/ejic.200900867

Mechanochemical Synthesis of Fe-Doped Apatite-Type Lanthanum Silicates

Tamara Kharlamova,*[a] Svetlana Pavlova,[a] Vladislav Sadykov,[a] Marina Chaikina,[b] Tamara Krieger,[a] Arcady Ishchenko,[a] Yurii Pavlyukhin,[b] Sergei Petrov,[b] and Christos Argirusis[c]

Keywords: Lanthanum / Silicates / Doping / Mechanical activation / Topochemistry

Apatite-type lanthanum silicates (ATLS) doped by Fe were prepared by using mechanical activation, and the effect of the nature of the dopant raw materials on the formation of ATLS was considered. Genesis of the formation of apatite was studied by XRD, IR, HRTEM, and Mössbauer and UV/Vis electron spectroscopy. The possibility of a partial substitution of Si in the apatite with a dopant and the mechanism of formation of ATLS in the course of mechanical activation depend on the dopant parent compound. The structural compatibility of La_2O_3, $La(OH)_3$, and apatite was shown to favor the rapid formation of apatite-type silicate by a cluster-topotactic mechanism during mechanical activation, and the formation of an amorphous ferrosilicate intermediate in the case of the $La(NO_3)_3/SiO_2$ precursor favors dopant incorporation into the apatite. However, dopant incorporation into the apatite structure was shown to be partially or fully hampered through milling when FeO(OH) and α-Fe_2O_3 are used as reagents. Using crystalline hydrates as dopant precursors was shown to result in the formation of apatite through a dissociative mechanism.

Introduction

Apatite-type lanthanum silicates (ATLS) belong to a wide class of isostructural compounds. Recently, they have attracted considerable interest as a new type of solid electrolyte possessing a high oxide ion conductivity at intermediate (500–800 °C) temperatures.[1] In contrast to the most traditional oxide electrolytes based on fluorite- and perovskite-type systems, where the ion conductivity is caused by jumping of oxygen atoms into vacancies, the ion conductivity in the apatite system is suggested to be mediated by interstitial oxygen atoms.[2–4] This is caused by peculiarities of the apatite structure that tolerates different structural defects such as cation vacancies and interstitial oxygen atoms.

In general, the hexagonal apatite structure can be presented by a crystallographic formula $M_{10}(RO_4)_6X_2$, where M = La^{3+}, Mg^{2+}, Ca^{2+}, etc.; R = Si^{4+}, Ge^{4+}, P^{5+} etc.; X = O^{2-}, OH^-, F^-, etc. It can be described as consisting of isolated tetrahedral RO_4 anions and M cations located in nine-coordinate *4f* or seven-coordinate *6h* sites (Figure 1). The seven-coordinate cations form channels along the *c* axis in which anions X are located. These anions, being oxide ions, are suggested to be responsible for the high anion conductivity in oxyapatites such as rare-earth silicates. However, only systems possessing a defect structure due to the presence of cation vacancies, for example $La_{9.33}Si_6O_{26}$, and/or oxygen excess, for example $La_{9.67}Si_6O_{26.5}$ and $La_9SrSi_6O_{26.5}$, show high ion conductivity, whereas stoichiometric systems such as $La_8Sr_2Si_6O_{26}$ have rather low conductivity.[5] This seems to be caused by some displacement of the oxide ion in channels from the center into an interstitial position for systems with cation vacancies and/or oxygen excess, which was shown by neutron diffraction studies. The latter along with atomistic modeling allows the interstitial mechanism of ion transport in apatite systems to be assumed.[2–4]

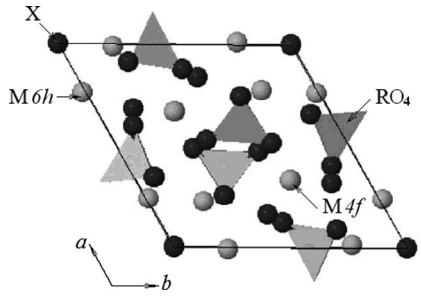

Figure 1. The apatite structure.

[a] Boreskov Institute of Catalysis SB RAS,
pr. Lavrentieva 5, 630090 Novosibirsk, Russian Federation
Fax: +7-383-3308056
E-mail: kharlamova@catalysis.ru
[b] Institute of Solid State Chemistry and Mechanochemistry of SB RAS,
Kutatetadze Street 18, 630128 Novosibirsk, Russian Federation
[c] Clausthal University of Technology,
38678 Clausthal-Zellerfeld, Germany

The amount of cation vacancies and oxygen excess can be controlled by doping, which allow improving transport properties of the ATLS. In this respect, different doping strategies such as lanthanum substitution and doping on the Si site were proposed to increase the oxygen ion conductivity of ATLS, samples doped on the Si site showing higher conductivity than comparable samples doped on the La site.[5,6] For some doped ATLS, the electrical conductivity close to that of Gd-doped ceria − one of the most perspective intermediate-temperature electrolytes − has been obtained.[7] This, along with high stability in both oxidizing and reducing condition, high transport numbers, and so on, make them promising materials for solid oxide fuel cells and other membrane technologies.

However, to promote the application of new electrolyte materials, inexpensive and simple preparation methods of ceramic powders based on ATLS, especially doped ones, should be developed. The conventional synthesis by solid-state reaction requires very long firing cycles (10–24 h, total duration up to 125 h) at temperatures in the range of 1200–1500 °C[2,3] and does not provide good control of the particle size and phase and stoichiometric heterogeneities. Lower synthesis temperatures allow nanocrystalline powders to be obtained, which play a crucial role in the preparation of functional ceramics.[8] This gives a rise to growing interest in the optimization of lower-temperature synthesis methods of ATLS ceramic powders.[9–12]

Recently, Rodriguez-Reyna et al. reported the synthesis of undoped apatite-type silicates by the mechanical milling of constituent oxides at room temperature.[11] Additionally, our recent results have shown that Al-doped ATLS can be easily prepared at room temperature through mechanochemical activation (MA) by using a high-power planetary ball mill, which allows a significant decrease in milling time.[12] On the basis of the obtained data the cluster-topotactic mechanism was suggested to explain the rapid formation of apatite during MA. This mechanism seems also to be suitable to explain the results obtained by Rodriguez-Reyna et al.[11,12] However, it is well known that MA is a complex process, with different experimental parameters such as raw materials, type of mill, rotation speed, ball-to-powder mass ratio, milling container, milling time, and type and size of the grinding media, determining final products of the activation and a mechanism of their formation.[13,14] Thus, in contrast to our and Rodriguez-Reyna et al. results, data on the milling of mixtures of La_2O_3 and SiO_2 to prepare silicates with an apatite structure obtained by Tzvetkov and Minkova include a complete amorphization of the reaction mixture after milling for 3 h and cannot be explained by the cluster-topotactic mechanism.[15]

This paper is devoted to the study of the synthesis of Fe-doped ATLS by using mechanochemical activation of mixtures containing Fe_2O_3, FeO(OH), $Fe(NO_3)_3/SiO_2$, or $Fe(HCOO)_3$ as the iron parent compound. The effect of the nature of the dopant raw materials on the formation of Fe-doped ATLS is considered. Phase, structural, and microstructural studies have been carried out to clarify the mechanism of formation of doped lanthanum silicates in mixtures with different Fe parent compounds.

Results and Discussion

Synthesis of Fe-Doped ATLS

La_2O_3–SiO_2–Fe_2O_3

The formation of ATLS has been studied in detail for the SiO_2–La_2O_3–Fe_2O_3 mixture corresponding to a stoichiometry of $La_{9.83}Si_{4.5}Fe_{1.5}O_{26}$. The results of the kinetic study are presented in Figures 2 and 3. According to XRD data, the start mixture contains La_2O_3, $La(OH)_3$, $La_2O_2CO_3$, and α-Fe_2O_3 (Figure 2). The latter possesses the corundum structure. Hexagonal La_2O_3 is the main lanthanum-containing phase. Admixtures of hexagonal $La(OH)_3$ and $La_2O_2CO_3$ are also present due to lanthanum oxide interaction with CO_2 and H_2O present in air.

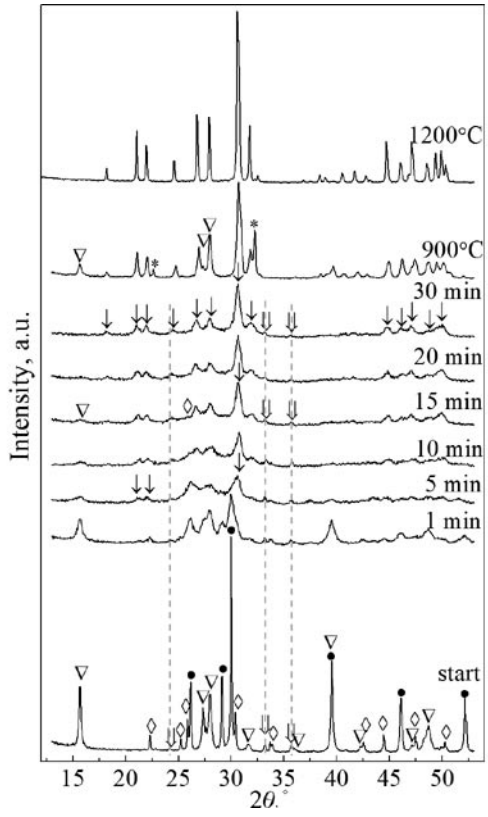

Figure 2. X-ray powder diffraction patterns of the SiO_2–La_2O_3–Fe_2O_3 mixture corresponding to a composition of $La_{9.83}Si_{4.5}Fe_{1.5}O_{26}$ before and after milling for different times and calcination at different temperatures: $La_2O_2CO_3$ (◇), apatite (↓); La_2O_3 (●), $La(OH)_3$ (∇), Fe_2O_3 (⇓), $LaFeO_3$ (*).

The IR spectra of the start mixture contains absorbance bands of Si–O–Si vibrations in silica at 552, 799, 950, 1093, and 1180 cm^{-1}, C–O vibrations in the $[CO_3]^{2-}$ anion in a crystalline carbonate at 746, 853, 1089, and 1464 cm^{-1}, and La–O–H vibrations at 645 and 3609 cm^{-1} (Figure 3). Absorbance bands of Fe–O vibrations in Fe_2O_3 are not clearly observed due to overlapping with a shoulder of the band of La–O vibrations in La_2O_3 at 400–550 cm^{-1}.

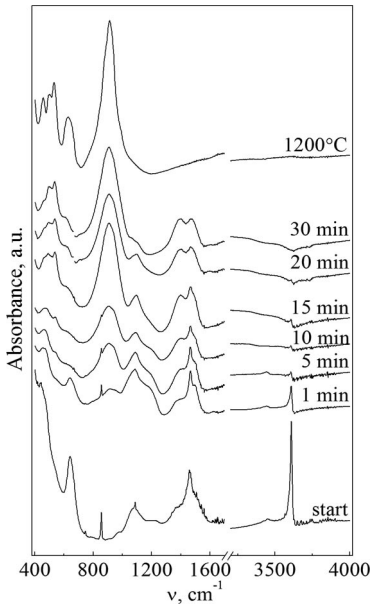

Figure 3. FTIR spectra of the SiO_2–La_2O_3–Fe_2O_3 mixture corresponding to a composition of $La_{9.83}Si_{4.5}Fe_{1.5}O_{26}$ before and after milling for different times and calcination at 1200 °C.

XRD and IR data show that an apatite phase forms in the course of the milling of the mixture (Figures 2 and 3). Indeed, in the IR spectrum of the mixture milled for 1 min a band at ca. 910 cm^{-1} attributed to asymmetric stretching vibrations of the Si–O band in isolated [SiO_4] tetrahedrons appears, indicating the beginning of the change in the Si local structure (Figure 3).[15,16] After milling for 5 min, the strongest and nonoverlapping reflections of apatite along with those of the starting compounds are observed in the corresponding XRD pattern (Figure 2). Virtually all apatite reflections are clearly observed in the XRD spectrum only after milling of the mixture for 15 min; however, reflections of starting $La(OH)_3$, $La_2O_2CO_3$, and Fe_2O_3 are still present in the pattern. The presence of starting compounds in the products of the mechanical activation even after 20 min milling is confirmed by analysis of the IR spectra, which show the bands of Si–O–Si vibrations in silica at 1093 and 1180 cm^{-1}, La–O–H vibrations at 645 and 3609 cm^{-1}, and C–O vibrations in the crystalline carbonate at 746, 853, 1089, and 1464 cm^{-1} (Figure 3). They practically disappear only after milling for 30 min, with broad bands at 1397 and 1476 cm^{-1} in the IR spectrum being caused by C–O stretching vibrations in surface CO_3 groups due to CO_2 adsorption after $La_2O_2CO_3$ decomposition.[17]

Though the apatite forms in the course of the milling of the SiO_2–La_2O_3–Fe_2O_3 mixture, Fe incorporation into the apatite structure is hampered. Thus, ferric oxide reflections are present in the XRD pattern of the mechanical activation product even after 30 min milling, being practically independent on the activation time (Figure 2). Besides, the absorbance in the region of 550–650 cm^{-1} of the spectra corresponds to Fe–O stretching vibrations in octahedral coordination in ferric oxide, rather than Fe–O stretching vibrations in isolated tetrahedrons.[16]

The formation of practically Fe-free ATLS is clearly shown by UV/Vis electron spectroscopy. The electron spectra of the products obtained after different milling time are presented in Figure 4. The spectrum of the start mixture contains bands at 11710 and 15350 cm^{-1} that correspond to d–d transition of Fe^{3+} in Fe_2O_3, where Fe is in the octahedral coordination. The band at 18260 cm^{-1} is apparently caused by metal–ligand charge transfer. Mechanical treatment results in the appearance of the strong bands at 25000 and 36000 cm^{-1}, which are typical for metal–ligand charge transfer of Fe^{3+} species in the octahedral complexes and clusters.[18] These bands can be caused by changing the Fe–O distance in Fe_2O_3 and its particle size decreases during the milling. At the same time, the character of the spectra in the region of d–d transitions is not substantially changed, indicating that the state of Fe does not vary during milling of the mixture. Thus, UV/Vis electron spectra confirm the formation of Fe-free apatite.

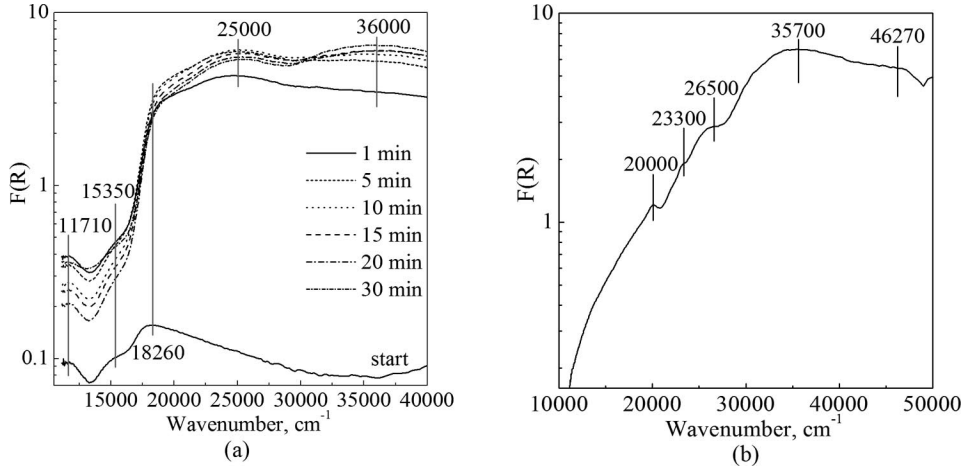

Figure 4. UV/Vis electron spectra of the SiO_2–La_2O_3–Fe_2O_3 mixture corresponding to a composition of $La_{9.83}Si_{4.5}Fe_{1.5}O_{26}$ before and after milling for different times (a) and calcination at 1200 °C (b).

Fe-doped apatite is formed after calcination of the 10 min activated SiO_2–La_2O_3–Fe_2O_3 mixture at 1200 °C for 6 h by the solid-state reaction of undoped apatite and $LaFeO_3$ that has been preliminarily formed after annealing the mechanically activated products at 900 °C (Figure 2). The sample annealed at 1200 °C is practically single-phase apatite with only minor (≈1 wt.-%) $LaFeO_3$ admixture. The structural parameters of the apatite (a = 9.778 Å; c = 7.260 Å) are greater than those of undoped ATLS and close to the parameters reported by Yaremchenko et al. for a sample of the same stoichiometry,[25] indicating lattice expansion due to Fe incorporation (Table 1). The incorporation of Fe into the apatite lattice is clearly shown by IR and UV/Vis electron spectroscopy data (Figures 3 and 4). The IR spectrum contains bands at 550–650 cm^{-1}, which is typical for Fe–O stretching vibrations in isolated [FeO_4] tetrahedrons.[16] In the corresponding electron spectrum three bands at 20000, 23300, and 26500 cm^{-1} attributed to d–d transition of Fe^{3+} in tetrahedral coordination are presented, and the band observed in the 30000–50000 cm^{-1} region is caused by metal–ligand charge transfer.[19,20] Thus, Fe does not incorporate into the apatite structure in the course of the MA of the SiO_2–La_2O_3–Fe_2O_3 mixture, but only after its subsequent calcination at temperatures >900 °C. However, using ceramic powders prepared by milling allows dense pellets of Fe-doped apatites to be obtained at a lower temperature and shorter time of sintering as compared with the conventional solid-state method.[21,22,25] Thus, the sintering of the activated mixtures at 1500 °C for 4 and 10 h results in a theoretical pellet density of 89 and 97%, respectively, whereas McFarlane et al. reported a theoretical pellet density of 70–76% for Fe-doped ATLS prepared by the conventional ceramic method and sintered at 1500 °C for 8 h.[21] In turn, for our samples, the sintering at 1600 °C for 4 h leads to a theoretical pellet porosity of >98–99%; Shaula reported a similar density for samples sintered at 1600 °C for 10–15 h.[22,25]

Table 1. Structural parameters of Fe-doped apatite-type lanthanum silicate calcined at high temperatures.

Sample stoichiometry	Unit-cell parameters of apatite			Reference
	a, Å	c, Å	Volume, Å^3	
$La_{9.83}Si_6O_{26}$	9.730	7.195	589.9	this study
	9.721	7.187	588.2	[6]
	9.725	7.190	588.9	[21]
$La_{9.83}Si_{4.5}Fe_{1.5}O_{26}$	9.778	7.260	601.1	this study
	9.773	7.260	600.5	[25]
$La_{9.83}Si_{5.5}Fe_{0.5}O_{26.5}$	9.748	7.219	594.1	this study
$La_{10}Si_5FeO_{26.5}$	9.761	7.240	597.4	this study
	9.757	7.255	598.1	[7]
	9.761	7.248	598.0	[21]

La_2O_3–SiO_2–FeO(OH)

The results of the activation of the SiO_2–La_2O_3–FeO(OH) mixture corresponding to the $La_{9.83}Si_{4.5}Fe_{1.5}O_{26}$ stoichiometry are presented in Figures 5, 6, and 7. According to XRD data, the only phases presented in the mixture activated for 15 min are an apatite and $LaFeO_3$ (Figure 5). Reflections of starting La_2O_3, $La(OH)_3$, $La_2O_2CO_3$, or FeO(OH) are not registered in the pattern. IR spectra confirm the practically complete consumption of parent compounds (Figure 6). There is only a weak band at 1100 cm^{-1} corresponding to Si–O–Si vibrations in silica, whereas the bands corresponding to La–O–H, C–O, and Fe–O or Fe–O–H vibrations in the parent $La(OH)_3$, $La_2O_2CO_3$, and

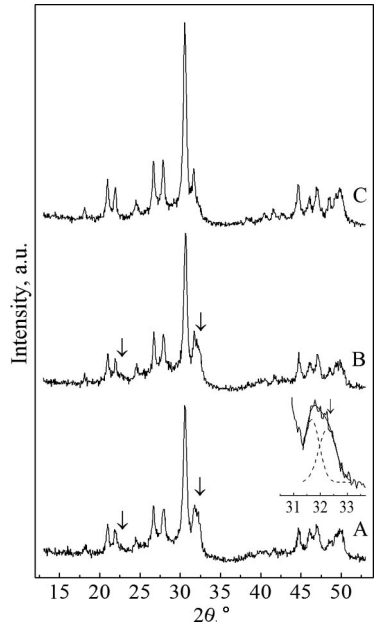

Figure 5. X-ray powder diffraction patterns of SiO_2–La_2O_3–FeO(OH) (A, B) and $Fe(NO_3)_3$/SiO_2–La_2O_3 (C) mixtures corresponding to a composition of $La_{9.83}Si_{4.5}Fe_{1.5}O_{26}$ after milling for 15 (A, C) and 30 min (B): $LaFeO_3$ (↓), apatite (unmarked reflections).

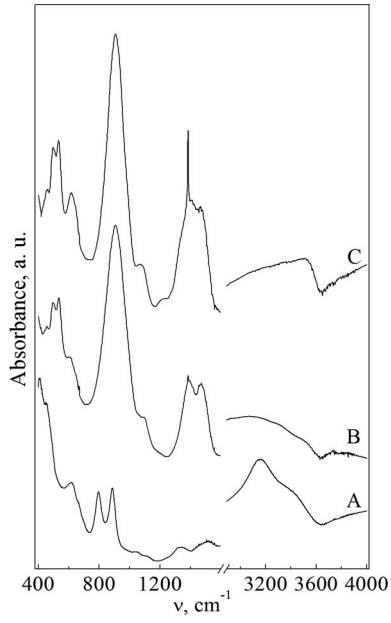

Figure 6. FTIR spectra of the parent FeO(OH) (A) and SiO_2–La_2O_3–FeO(OH) (B), and $Fe(NO_3)_3$/SiO_2–La_2O_3 (C) mixtures corresponding to a composition of $La_{9.83}Si_{4.5}Fe_{1.5}O_{26}$ after activation for 15 min.

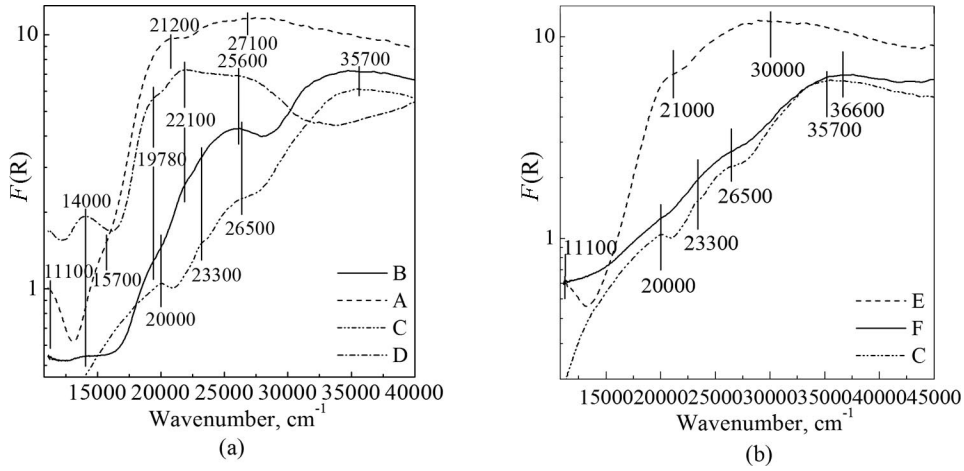

Figure 7. UV/Vis electron spectra: (a) FeO(OH) (A), SiO_2–La_2O_3–FeO(OH) mixture corresponding to a composition of $La_{9.83}Si_{4.5}Fe_{1.5}O_{26}$ activated for 15 min (B), $La_{9.83}Si_{4.5}Fe_{1.5}O_{26}$ calcined at 1200 °C for 5 h (C), and $LaFeO_3$ (D); (b) $Fe(NO_3)_3/SiO_2$ precursor (E) and $Fe(NO_3)_3/SiO_2$–La_2O_3 mixture corresponding to a composition of $La_{9.83}Si_{4.5}Fe_{1.5}O_{26}$ activated for 15 min (F).

FeO(OH), respectively, are not observed in the spectrum. The absorbance in the region of 550–675 cm^{-1} is caused by a superposition of Fe–O stretching vibrations in octahedral and tetrahedral coordination, indicating the presence of Fe in both $LaFeO_3$ and apatite.[16]

Electron spectra of the mechanically activated products milled for 15 min further confirm the complete consumption of the parent FeO(OH) in the course of milling and distribution of Fe^{3+} among the octahedral and tetrahedral sites (Figure 7a). The d–d transition bands (11100, 15700, 21200, and 27100 cm^{-1}) typical for octahedral coordinated Fe^{3+} in the start FeO(OH) disappear after MA (Figure 7a, spectrum B), whereas another bands also attributed to d–d transitions of Fe^{3+} in octahedral coordination appear in the spectrum at ca. 11000 and 14000 cm^{-1}. Taking into account the XRD and IR data, they can be attributed to d–d transitions of Fe^{3+} in $LaFeO_3$. However, the spectrum of the activated mixture is different from that of the individual $LaFeO_3$ (Figure 7a, spectrum D), which is caused by the simultaneous presence of d–d transition bands of tetrahedral coordinated Fe^{3+}. In so doing, in the mechanically activated products after 15 min milling Fe is mainly included in the perovskite and longer milling does not lead to the incorporation of an extra amount of Fe in the apatite (Figure 5). The presence of $LaFeO_3$ perovskite seems to be caused by its formation being kinetically more preferable than Fe incorporation into the apatite during the milling of the SiO_2–La_2O_3–FeO(OH) mixture in contrast to SiO_2–La_2O_3–$Al(OH)_3$ when there is some $LaAlO_3$ perovskite observed in the mechanically activated products mainly due to limited solubility of Al in the apatite.[12,13] The primary incorporation of Fe into the apatite occurs only after calcination of the mechanically activated products at 1200 °C, though some amount of $LaFeO_3$ still remains.

$Fe(NO_3)_3$/SiO_2–La_2O_3

Apatite Formation During Mixture Activation

The data on the milling of the mixture containing $Fe(NO_3)_3/SiO_2$ as the Fe precursor are shown in the Figures 5–8. The XRD (Figure 5) and HRTEM (Figure 8) data reveal that the 15 min MA of the mixture corresponding to the $La_{9.83}Si_{4.5}Fe_{1.5}O_{26}$ stoichiometry results in the formation of a practically single-phase apatite doped with Fe as EDX analysis indicates (Figure 8). According to microscopy data, the crystalline apatite nanoparticles of 10–70 nm form micron-sized agglomerates. Some amorphous ferrosilicate phase covering the crystalline apatite particles is also visible in the HRTEM images (Figure 8). A similar amorphous aluminosilicate phase was previously registered for Al-doped ATLS formed in the course of milling the La_2O_3–SiO_2–$Al(OH)_3$ mixture.[12,23]

IR data confirm the practically complete consumption of parent compounds and the formation of Fe-doped ATLS (Figure 6). Thus, bands of the La–O–H (645, 3609 cm^{-1}) and C–O (746, 853, 1089, 1464 cm^{-1}) vibrations in parent $La(OH)_3$ and $La_2O_2CO_3$, respectively, are not observed in the spectrum of the mechanical activation product. A band with maximum at 910 cm^{-1} and those with maxima at 493 and 536 cm^{-1} are attributed to Si–O vibrations in isolated [SiO_4] tetrahedrons in apatite. The absorbance at the region from 580 to 650 cm^{-1} is caused by the Fe–O stretching vibrations in isolated [FeO_4] tetrahedrons.[16] Nonintensive bands at 1064 and 1233 cm^{-1} differ from Si–O vibrations in silica and are broadened and shifted to low-frequency range. This can be caused by the presence of Si–O–Fe bands along with those of Si–O–Si.[24] This correlates with TEM data, indicating some amorphous ferrosilicate phase. The strong band at 1385 cm^{-1} presented in the spectra of the activated mixture is caused by N–O vibrations in the NO_3 group.

UV/Vis electron spectra also confirm the presence of Fe in the tetrahedral coordination (Figure 7b). Thus, three broad bands can be observed in the region between 20000 and 30000 cm^{-1}, which can be attributed to d–d transitions for Fe^{3+} in tetrahedral coordination.[18–20] These bands at 20000, 23300, and 26500 cm^{-1} become more clearly observed after calcination of the sample.

To provide insight into the formation of Fe-doped ATLS in the course of $Fe(NO_3)_3/SiO_2$–La_2O_3 milling, for the mix-

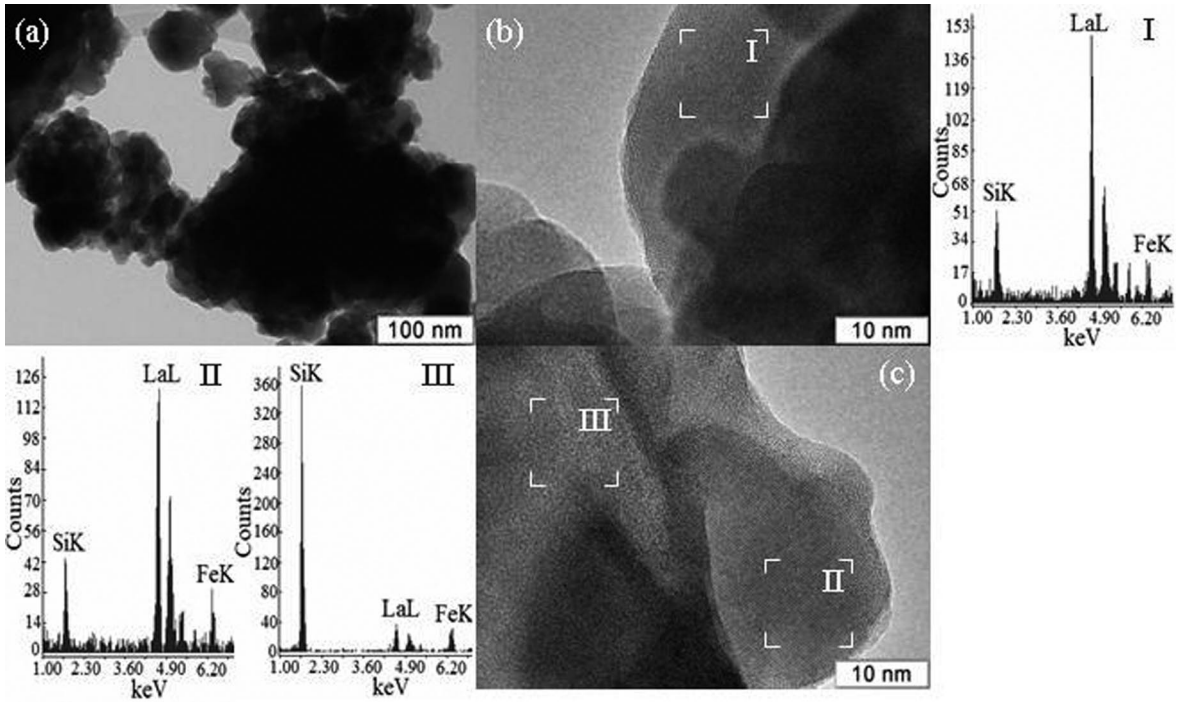

Figure 8. Typical TEM micrographs of the $Fe(NO_3)_3/SiO_2$–La_2O_3 mixture corresponding to a composition of $La_{9.83}Si_{4.5}Fe_{1.5}O_{26}$ activated for 15 min (a, b, and c) and EDX data for the corresponding particles (I, II, and III).

ture corresponding to $La_{9.83}Si_{5.5}Fe_{0.5}O_{26.5}$, a kinetic study has been carried out by using IR and Mössbauer spectroscopy. The IR spectrum of the start mixture contains bands of Si–O vibrations in silica, La–O and La–O–H vibrations in lanthanum oxide and hydroxide, C–O vibrations in crystalline $La_2O_2CO_3$, and N–O vibrations in the NO_3 group (vide supra; Figure 9a). Activation for 1 min results in a broadening and low-frequency shifting of Si–O vibration bands from 1090 to 1070 cm^{-1} due to the appearance of an Si–O–Fe vibration, indicating the formation of Fe-silicate.[24] Additionally, the band at 911 cm^{-1} can be already observed, indicating the start of the formation of the Si local environment typical for orthosilicates. The clearly observed reduction of bands of the N–O vibration at 1387 cm^{-1} and the C–O vibration at 851 and 1083 cm^{-1} and the appearance of broad bands at 1400 and 1480 cm^{-1} reflect a decomposition of crystalline nitrate and carbonate, respectively. The appeared bands correspond to C–O vibrations in a surface carbonate. It should be also noted that bands of La–O–H vibrations are still present in the spectrum of the mixture activated for 1 min.

Further milling results in the appearance of strong bands typical for Si–O vibration in apatite-type silicate at 492, 439, and 910 cm^{-1} accompanied by the disappearance of La–O–H and C–O vibrations bands in $La(OH)_3$ and $La_2O_2CO_3$, respectively. Besides, bands of Fe–O vibrations at 615 and 652 cm^{-1} typical for isolated $[FeO_4]$ tetrahedrons are also observed in the spectrum of the mixture activated for 5 and 15 min. The band of the N–O vibration in the NO_3 group at 1387 cm^{-1} does not completely disappear even after 15 min activation. However, the intensity of this band significantly

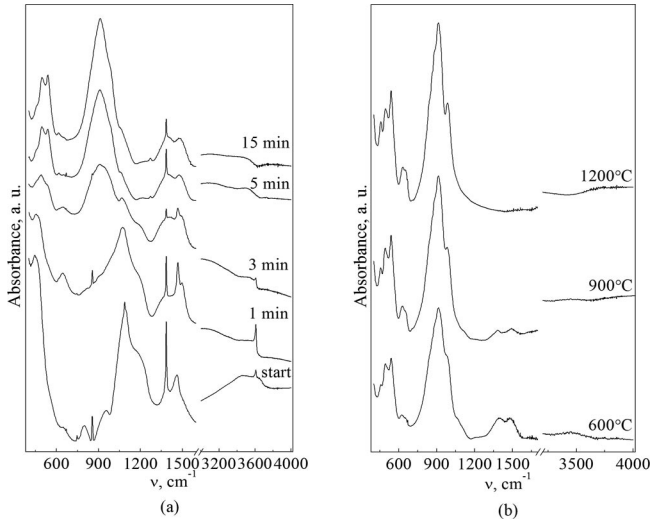

Figure 9. FTIR spectra of the $Fe(NO_3)_3/SiO_2$–La_2O_3 mixture corresponding to a stoichiometry of $La_{9.83}Si_{5.5}Fe_{0.5}O_{26.5}$ after milling for different times (a) and subsequent calcination of the sample milled for 15 min at different temperatures (b).

decreases in comparison with the inactivated mixture due to nitrate decomposition. Weak bands at ca. 1060 and 1217 cm^{-1} observed in the spectrum after 15 min MA indicate the presence of some amount of Fe-silicate.

Mössbauer spectroscopy data for the mixture after 1–15 min MA are presented in Figure 10a. The spectra of the mechanically activated products are characterized by wide

lines, which make data interpretation difficult. Such widening seems to be caused by a high density of point defects and dislocations typical for samples after milling, as well as by a wide range of Mössbauer nuclei states in the crystal due to variation of their local atomic and electronic environment. Nevertheless, Mössbauer spectra provide additional information about evolution of the local environment of Fe during activation. Thus, the spectrum of the mixture after milling for 1 min contains two lines that can be decomposed into two doublets with isomer shift (IS) corresponding to Fe^{3+} in octahedral coordination (Table 2). The quadrupole splitting indicates a distortion of the local octahedral symmetry. The doublet with IS = 0.351 mm/s seems to be caused by iron cations in a silicate.

Spectra of the mixture after the longer activation also contain the doublet with average IS of 0.239–0.292 mm/s. The doublet in the spectrum after activation for 3 min is symmetric and is not decomposed during spectrum processing, IS being 0.284 mm/s (Table 2). This corresponds to Fe^{3+} in tetrahedral coordination.[24] The quadrupole splitting points a distortion of the local tetrahedral symmetry. Besides, the strong line widening indicates that there are a lot of structural defects in the activated sample and iron ions can be distributed in sites having slightly different chemical environments. Taking the IR data into account, it can be assumed that amorphous Fe-silicate containing Fe in tetrahedral coordination is formed during the first milling minutes.

The spectra of the mixture activated for 5 and 15 min contain an asymmetric doublet (Figure 10a). However, their processing revealed only one Fe^{3+} state with IS of 0.241 and 246 mm/s for spectra after 5 and 15 min milling, respectively, which correspond to iron ions in tetrahedral coordination (Table 2). Such a result of spectrum processing can be caused by a strong line widening due to the presence of a lot of defects and tetrahedral coordinated Fe^{3+} in different states. Note, that IS of 0.22–0.29 mm/s is reported for Fe^{3+} ions in tetrahedral coordination in zeolites,[24] whereas Shaula and Yaremchenko report an IS value of 0.11–0.18 mm/s for Fe^{3+} ions in tetrahedral coordination in apatite-type silicates calcined at 1500–1600 °C.[22,25] Nevertheless, some shifting of IS to lower values indicates a change in the local atomic and/or electronic environment of the

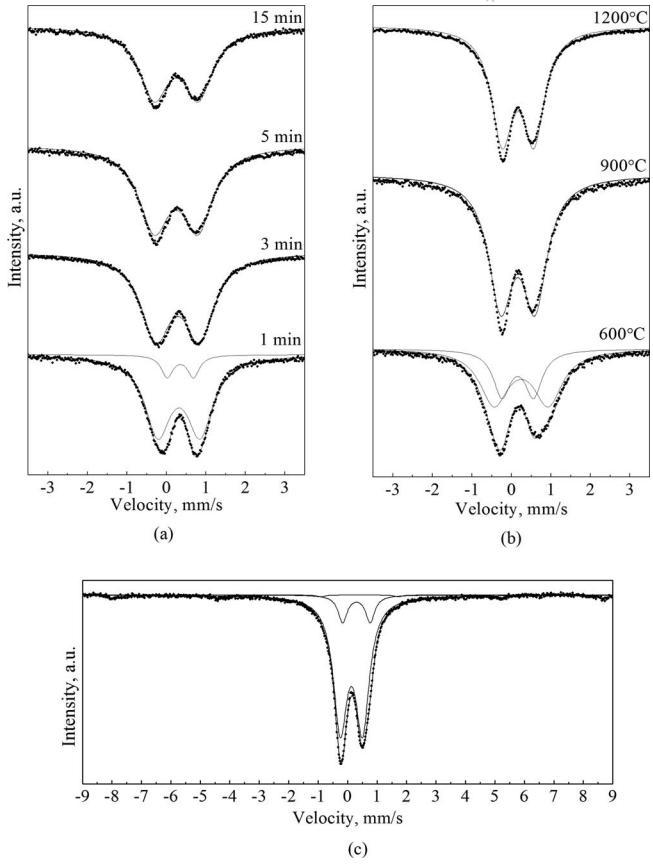

Figure 10. Mössbauer spectra of the $Fe(NO_3)_3/SiO_2$–La_2O_3 mixture corresponding to stoichiometries of $La_{9.83}Si_{5.5}Fe_{0.5}O_{26.5}$ (a, b) and $La_{10}Si_5FeO_{26.5}$ (c): (a) the mixture after milling for different times; (b) the mixture milled for 15 min after subsequent calcination at different temperatures; (c) the mixture calcined at 1200 °C.

Fe^{3+} ions. This also agrees with IR data (Figure 9), clearly showing the presence of a part of Fe^{3+} ions in isolated $[FeO_4]$ tetrahedrons in the spectrum of a mixture activated for 5 min and longer (vide supra). Thus, using $Fe(NO_3)_3/SiO_2$ as the Fe precursor favors the formation of the Fe-doped ATLS already in the course of MA, though according to IR and Mössbauer data, some Fe-silicate is still present in the mixture milled for 15 min.

Table 2. Mössbauer data for samples of $La_{9.83}Si_{5.5}Fe_{0.5}O_{26.5}$ and $La_{10}Si_5FeO_{26.5}$ stoichiometry.

Treatment	Average IS, mm/s	Iron state	IS, mm/s	Width, mm/s	QS, mm/s	I, %
Activation for 1 min	0.344	Fe^{3+}, CN = 6	0.316	0.791	1.069	88
		Fe^{3+}, CN = 6	0.351	0.360	0.664	12
Activation for 3 min	0.292	Fe^{3+}, CN = 4	0.284	0.898	1.104	100
Activation for 5 min	0.239	Fe^{3+}, CN = 4	0.241	0.931	1.103	100
Activation for 15 min	0.250	Fe^{3+}, CN = 4	0.246	0.890	1.116	100
Calcination at 600 °C	0.176	Fe^{3+}, CN = 4	0.244	0.871	1.372	66
		Fe^{3+}, CN = 4	0.158	0.528	0.799	34
Calcination at 900 °C	0.155	Fe^{3+}, CN = 4	0.161	0.740	0.869	100
Calcination at 1200 °C	0.156	Fe^{3+}, CN = 4	0.165	0.655	0.804	100
Calcination at 1200 °C[a]	0.167	Fe^{3+}, CN = 4	0.129	0.565	0.755	84
		Fe^{3+}, CN = 5	0.300	0.370	0.935	12
		Fe^{3+}, CN = 6[b]	0.390	0.287	–0.014	4

[a] $La_{10}Si_5FeO_{26.5}$ sample stoichiometry. [b] H = 16.569 T.

Calcination of the Activation Product

The subsequent calcination of the products after 15 min MA leads to completion of the synthesis of Fe-doped apatite and ordering of its structure. Thus, according to IR data, the calcination of the mechanical activation product at 600 °C results in the disappearance of the bands of the N–O vibration and a decrease in the intensity of the C–O vibrations of surface carbonates (Figure 9b). This shows that the starting nitrate is completely decomposed, whereas some carbonates are still present in the sample. In addition, a shift to a higher wavenumber and an increase in the intensity of the Fe–O vibrations bands of isolated [FeO_4] tetrahedrons are observed. The appearance of the band at 984 cm^{-1} indicates some splitting of Si–O vibrations in apatite due to lowering of the [SiO_4] group symmetry to C_1 or C_2 because of strong local distortion.[16,26] Calcination of the sample at 900–1200 °C causes disappearance of bands of C–O vibrations in the surface carbonate and Si–O–Fe vibrations in Fe-silicates. This is accompanied by an increase in the band intensity, a decrease in the band broadening, and further splitting of Si–O vibrations as well as shifting and an increase in the intensity of the Fe–O vibration bands, which is caused by structure ordering in crystalline apatite and complete Fe incorporation into the structure during the calcination. The analysis of the unit cell values for diffraction patterns of the $La_{9.83}Si_{5.5}Fe_{0.5}O_{26.5}$ sample calcined at 1200 °C gives parameters a = 9.748 Å and c = 7.219 Å, indicating lattice expansion due to Fe incorporation (Table 1).

The calcination of the mechanically activated products also results in evolution of the Mössbauer spectra (Figure 10b). The spectrum of the sample calcined at 600 °C contains an asymmetric doublet with an average IS of 0.176 mm/s, which is similar to the spectra of the mechanically activated products after 5 and 15 min milling (Table 2). However, the bands become narrow and spectrum processing reveals two doublets with IS of 0.244 and 0.158 mm/s, corresponding to Fe^{3+} ions in tetrahedral coordination. The doublet with IS = 0.244 mm/s is assumed to be caused by ions in the amorphous Fe-silicate and the doublet with IS = 0.158 mm/s is ascribed to ions in the apatite structure. Calcination at 900–1200 °C leads to further bandwidth narrowing and shifting of the average IS value of the doublet to 0.155–0.156 mm/s. In spite of the asymmetry of the doublet, spectra processing gives only one doublet with IS = 0.161 and 0.165 mm/s for the samples calcined at 900 and 1200 °C, respectively (Table 2). This corresponds to Fe^{3+} ions in tetrahedral coordination in the apatite lattice.

The asymmetry of the doublet in the spectra of samples calcined at 900 and 1200 °C can be caused by iron ions present in a state that cannot be revealed during processing of the spectrum for a strong line widening, because the iron ion distribution among the sites has slightly different environments. This is indirectly confirmed by Mössbauer data for the $La_{10}Si_5FeO_{26.5}$ sample (a = 9.761 Å, c = 7.240 Å), which was also synthesized by MA of $Fe(NO_3)_3/SiO_2$–La_2O_3 followed by calcination at 1200 °C (Table 1). The corresponding spectrum presented in Figure 10c contains two intense bands and some bands of low intensity. Spectrum processing revealed two doublets with IS = 0.129 and 0.300 mm/s and a sextet with IS = 0.390 mm/s (Table 2). The latter corresponds to Fe^{3+} ions in octahedral coordination, which can be caused by the presence of trace amounts of $LaFeO_3$ (0.49 wt.-%) in the sample due to limitation of the extension of a solid solution with the apatite structure.[12] However, the $LaFeO_3$ phase was not detected by other methods such as XRD, IR, and UV/Vis electron spectroscopy for this sample, which does not rule out the presence of octahedron-coordinated Fe in the apatite structure. The doublet with IS = 0.129 mm/s corresponds to Fe^{3+} ions in tetrahedral coordination in the apatite lattice, whereas the doublet with IS = 0.300 mm/s is ascribed to five-coordinate Fe^{3+} ions in apatite. The latter is assumed to be caused by the presence of interstitial oxygen atoms, and this was earlier reported by Shaula on the basis of Mössbauer data.[22]

Using ceramic powders prepared this way allows ceramic pellets to be made that have a theoretical density of ca. 90% after sample sintering at 1450 °C for 2 h. In so doing, good component mixing and Fe incorporation into the apatite structure before pellet sintering favors ceramic homogeneity.

La_2O_3–SiO_2–$Fe(HCOO)_3$ Mixture Activation

Results of the SiO_2–La_2O_3–$Fe(HCOO)_3$ mixture activation are presented in Figures 11–14. According to XRD data, after milling for 1 min the mixture contains $La(OH)_3$, La_2O_3, and $La_2O_2CO_3$ phases, and both $La(OH)_3$ and La_2O_3 are the main La-containing phases (Figure 11). Re-

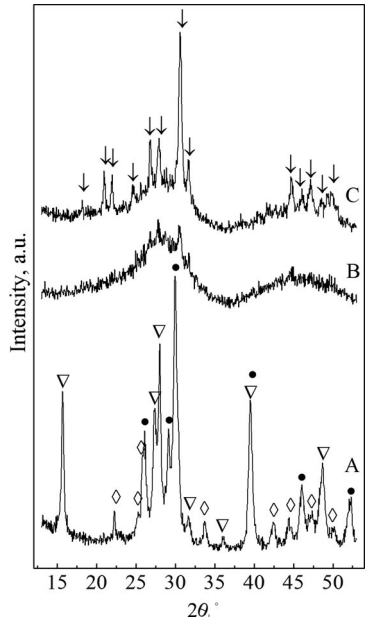

Figure 11. X-ray powder diffraction patterns of the SiO_2–La_2O_3–$Fe(HCOO)_3$ mixture corresponding to a composition of $La_{9.83}Si_{4.5}Fe_{1.5}O_{26}$ after milling for 1 (A), 15 (B), and 30 min (C): $La_2O_2CO_3$ (◇), apatite (↓),La_2O_3 (●), $La(OH)_3$ (∇).

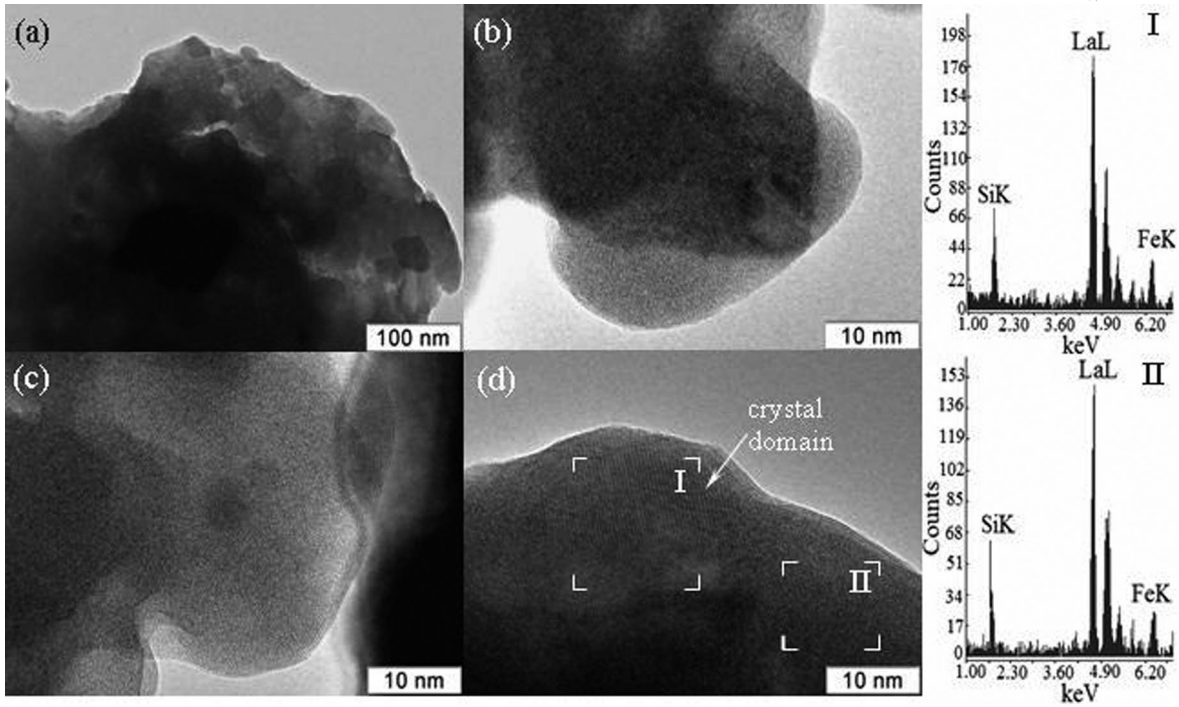

Figure 12. Typical TEM micrographs of the SiO_2–La_2O_3–$Fe(HCOO)_3$ mixture corresponding to a composition of $La_{9.83}Si_{4.5}Fe_{1.5}O_{26}$ after milling for 15 min (a, b, c, and d) and EDX data for the corresponding particles (I and II).

flections of $Fe(HCOO)_3$ are not observed in the pattern. The following mixture activation up to 15 min results in the formation of amorphous products: in the corresponding XRD pattern there are two broad peaks at the regions of 2θ from 18 to 35° and from 38 to 55°. Several weak peaks assigned to the reflection of the apatite phase can be singled out in the first region, indicating the beginning of the formation of apatite. All apatite reflections are clearly observed in the XRD pattern after milling of the mixture for 30 min. However, broad peaks caused by the presence of the amorphous phase are still observed in the pattern as well, being appreciably smaller.

TEM study confirms the formation of the intermediate amorphous product during activation of the mixture (Figure 12). Amorphous particles are mainly observed in the micrographs of the sample milled for 15 min. According to EDX analysis of the particles, this phase simultaneously consists of La, Si, and Fe (Figure 12b,c). In some micrographs, crystal domains are observed that correlate with the XRD data, suggesting the beginning of the formation of apatite (Figure 12c).

IR data also show the formation of the intermediate amorphous phase and give information on changing of the Si local structure. In the spectrum after 15 min activation, the strong band at 910 cm^{-1} corresponding to the Si–O stretching vibrations in isolated [SiO_4] groups is observed (Figure 13). This band is rather typical for an amorphous silicate than for the crystalline apatite.[12,13,16] Besides, only one broad band at ca. 509 cm^{-1} is observed in the region of Si–O deformation vibrations. This reflects that the isolated [SiO_4] tetrahedrons are not rigidly bounded in a regular lattice. In the region of O–H stretching vibrations, bands apparently caused by Si–O–H group vibrations are observed, which also indirectly confirms the formation of amorphous silicate.

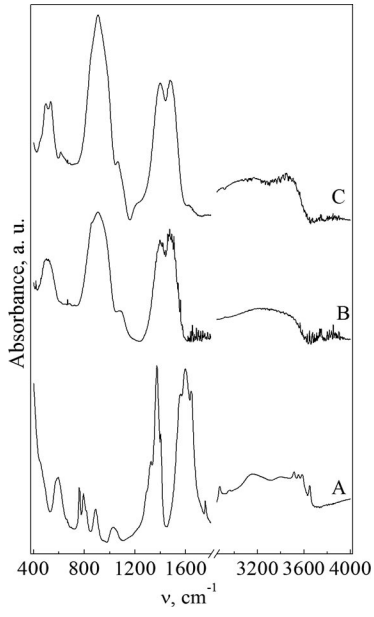

Figure 13. FTIR spectra of the parent $Fe(HCOO)_3$ (A) and the SiO_2–La_2O_3–$Fe(HCOO)_3$ mixture corresponding to a composition of $La_{9.83}Si_{4.5}Fe_{1.5}O_{26}$ after milling for 15 (B) and 30 min (C).

According to IR data, milling for 15 min also results in formate decomposition to form carbonates (bands in the region of 1250–1600 cm^{-1}). However, there are no charac-

teristic bands of Fe–O vibration in $[FeO_4]$ or $[FeO_6]$ in the spectra. This can be caused by the presence of Fe in the second coordination sphere of Si (the bond like Si–O···Fe^{3+}) in the formed amorphous silicate.

The IR spectrum of the mixture after activation for 30 min contains strong bands typical for Si–O vibrations in isolated $[SiO_4]$ groups of ATLS (497, 534, 908 cm^{-1}).[11] There is also a wide band in the region of 3300–3650 cm^{-1} and a band at 1618 cm^{-1} assigned to O–H vibration in water. The band at 613 cm^{-1} can be assigned to Fe–O vibrations in isolated $[FeO_4]$ tetrahedrons. However, a part of Fe seems to be present in an amorphous Fe-silicate precursor (1063, 1220 cm^{-1}).[16] It seems that for complete synthesis of the target compound, longer mechanochemical treatment should be used.

The UV/Vis electron data do not contradict the corresponding IR data, suggesting the presence of Fe in the second coordination sphere of Si. The UV/Vis electron spectrum of the 15 min activated mixture is characterized by absorption near 11000 cm^{-1} caused by Fe^{3+} d–d transition and strong absorption in the region of 30000–40000 cm^{-1} caused by metal–ligand charge transfer (Figure 14). There is also a weak band at 21200 caused by Fe^{3+} d–d transition. The band near 11000 cm^{-1} reflects the presence of Fe^{3+} in octahedral coordination. However, weak bands at 21200 cm^{-1} can be caused by d–d transitions of Fe^{3+} in tetrahedral coordination.[19,20]

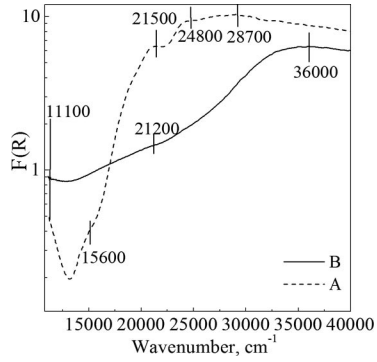

Figure 14. UV/Vis electron spectra of $Fe(HCOO)_3$ (A) and SiO_2–La_2O_3–$Fe(HCOO)_3$ (B) mixture corresponding to a composition of $La_{9.83}Si_{4.5}Fe_{1.5}O_{26}$ after milling for 15 min.

The Mechanism of Formation of Apatite

Mechanical activation causes a broad spectrum of parallel processes such as grinding, generation of defects in the solids, compaction to form molecular-dense aggregates, chemical interaction of the components, sometimes, accompanied by heating and melting of the reacting mixture, and so on.[13] In so doing, the chemical interaction between solids is greatly accelerated in comparison with thermally activated reactions due to facilitating mass transfer that occurs by means of diffusion on surface of particles and the bulk of quite small defect particles of the components.[14] A number of studies are devoted to the mechanism of component interaction in the course of MA.[14,27,28]

The most prevailing models for the formation of compounds in the course of MA engage the interaction of components through mixing on the atom-ionic level.[27,28] There is also work based on another mechanisms of mechanochemical synthesis depending on the structure and physicochemical properties of the starting and target compounds. Thus, for the synthesis of phosphorus apatite, along with the dissociative mechanism including mixing on the atom-ionic level, plastically deformative and cluster-topotactic mechanisms have been suggested by Chaikina.[14] When structures of the starting compound and the product of activation are different, MA results in the destruction of the starting compounds to form the amorphous state of the mixture. In this case, the interaction of the components occurs by a dissociative mechanism through component mixing on the atom-ionic level followed by crystallization of the target product from the amorphous phase.

When the structures of the starting compound and the product of MA are identical, the interaction of the components can occur by the plastically deformative mechanism without destruction of the initial matrix by means of a plastic strain, particularly, the deformation of the slide that unseals structure planes of the initial matrix, favoring substitution and combination reactions to form a target product. This mechanism is characterized by the disruption of only the distant atomic order of the starting compound, whereas the structural matrix and its local atomic order remain during MA.

Finally, the interaction of the mixture components can occur by the cluster-topotactic mechanism when structures of the starting compound and the product of MA are similar. This mechanism includes oriented interaction when all or part of the crystal structure of the initial component is retained in the target product. For a topotactic transformation, a 3D similarity between the structures of a starting material and a product is important but not obligatory, and even the compositions may differ radically.[29,30] Such interaction of the components during milling occurs without the formation of an amorphous state of the mixture and proceeds faster than interaction of the same components through the plastically deformative or dissociative mechanisms.[14]

The data obtained in this work show that the formation of ATLS can occur by the cluster-topotactic or dissociative mechanism depending on the dopant parent compound. The dissociative mechanism is realized in the case of the MA of the SiO_2–La_2O_3–$Fe(HCOO)_3$ mixture, which leads to the destruction of the starting and intermediate compound lattice and to the formation of the amorphous state of the mixture followed by the crystallization of ATLS (Figures 11 and 12). This seems to be caused by the presence of appreciable amounts of H_2O formed from $Fe(HCOO)_3$ crystalline hydrate in the reaction space. Strong hydration of ions in the course of milling favors the destruction of structures of the mixture components, resulting in the formation of apatite through a dissociative mechanism.[14]

For all other experiments, the mechanochemical reaction of the apatite synthesis does not involve the amorphization of the mixture (Figures 2 and 8). The presence of crystalline

Table 3. Structural parameters of La_2O_3, $La(OH)_3$, and apatite-type lanthanum silicate.

Compound	Structural formula	CN (La)	Lattice	Unit cell dimensions		Space		Volume	
				a, Å	*c*, Å	*α*, °	*γ*, °	Group	A^3
La_2O_3	La_2O_3	7	hexagonal	3.937	6.130	90	120	$P\bar{3}2/m1$	82.3
$La(OH)_3$	$La_2(OH)_6$	9	hexagonal	6.547	3.854	90	120	$P6_3/m$	143.1
Apatite	$La_{9.83}(SiO_4)_6O_2$	7, 9	hexagonal	9.719	7.187	90	120	$P6_3/m$	587.9

phases in the course of milling as well as the formation of $La(OH)_3$ preceded[12] and accompanied by the relatively rapid formation of apatite (Figures 2, 3, and 9) suggest the possibility of the cluster-topotactic mechanism.[14] The structural similarities of La_2O_3, $La(OH)_3$, and apatite crystallized in the lattice of hexagonal symmetry (Table 3) also argue in favor of this mechanism. The relationship between the structures can be deduced by comparing the individual projections down [001] and [100] in the appropriate orientations (Figures 15 and 16). These structures have a relatively unchanged cation framework of hexagonal close packing, though an anion sublattice undergoes appreciable changes, especially for apatite. Such a structure variation including cation rigidity in the course of the topotactic reactions is usual for systems with large cations.[29]

In the case of the formation of ATLS from lanthanum oxide, the structure of lanthanum hydroxide as an intermediate allows the formation of apatite through the topotactic mechanism. Thus, the coordination number (CN) of lanthanum in lanthanum oxide is 7, whereas there are seven- and nine-coordinate lanthanum cations in the apatite (Table 3). Lanthanum oxide hydration leads to an increase in the CN of lanthanum from 7 to 9. This is also accompanied by lattice expansion in the *a* and *b* dimensions and its contraction in the *c* dimension (Table 3). Subsequent acid–base interaction between the lanthanum hydroxide and silica or intermediate amorphous silicate results in the incorporation of silicon into the structure to form the apatite structure. This leads to the additional lattice expansion in three dimensions and to a decrease in the CN from 9 to 7 for 64% of the lanthanum cations (Table 3).

However, when the cluster-topotactic mechanism is realized, the introduction of Fe into the apatite structure in the course of the milling depends on the nature of the dopant parent and is connected with the formation of intermediate amorphous ferrosilicate. Thus, the activation of only the $Fe(NO_3)_3/SiO_2$–La_2O_3 mixture (Figure 9) accompanied by the formation of intermediate ferrosilicate results in the formation of doped ATLS during the activation. Previously, the similar formation of doped apatite accompanied by the formation of intermediate aluminosilicate was revealed for a Al-doped system in the course of milling the SiO_2–La_2O_3–$Al(OH)_3$ mixture.[12]

In contrast to the mixtures containing $Al(OH)_3$[12] and $Fe(NO_3)_3/SiO_2$, the presence of chemically inert Fe_2O_3 of the corundum structure in the activated mixture results in the formation of the undoped apatite (Figure 4) through the cluster-topotactic mechanism. Ferric oxide remains practically unchanged, playing the role of milling agents (Figures 2 and 4).

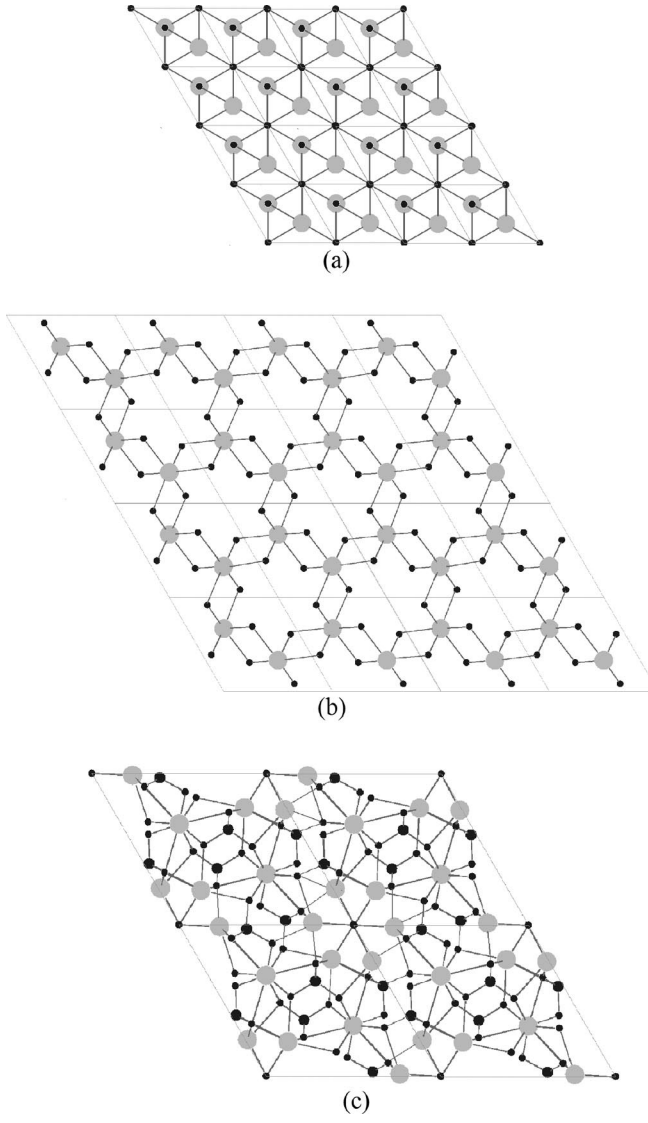

Figure 15. [001] projections of La_2O_3 (a), $La(OH)_3$ (b), and apatite (c) structures.

The activation of the SiO_2–La_2O_3–FeO(OH) mixture results in the complete consumption of FeO(OH) (Figures 5 and 7). However, only a small part of Fe is introduced in the apatite lattice, and Fe is mainly present in the form of $LaFeO_3$ as UV/Vis electron data indicate (Figure 7). In this case, the mechanochemical equilibrium seems to set in between Fe-doped ATLS and $LaFeO_3$ as a result of the competition of the structural types for deficient reagent.[13]

Thus, the rapid formation of ATLS through the topotactic acid–base reaction in the course of milling is favored by

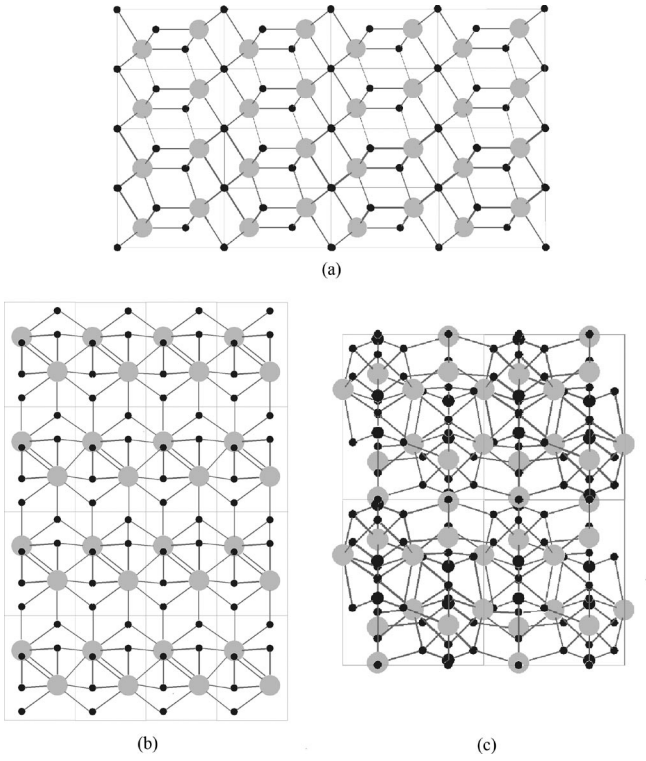

Figure 16. [100] projections of La_2O_3 (a), $La(OH)_3$ (b), and apatite (c) structures.

the similarity of the structures of La_2O_3, $La(OH)_3$ and apatite, whereas the incorporation of the dopant into the apatite structure on the Si site during milling implies the formation of intermediate amorphous silicate, for example, ferro- or aluminosilicate. This requires the use of dopant precursors possessing hardness close to silica or the rapid transforming into a reactive intermediate to provide its preliminary interaction with silica.[13] The use of a precursor having hardness higher than silica and low reactivity leads to its interaction with La_2O_3 and/or other mixture components having a proper hardness to form byproducts, for example, $LaFeO_3$ in the case of FeO(OH), or does not provide its interaction at all, for example, in the case of α-Fe_2O_3. In so doing, the presence of water in the reaction space favors chemical interaction in the course of milling, including acid–base interactions between the mixture components and intermediates.[14] However, an appreciable amount of water can result in the destruction of structures of the mixture components, affecting the mechanism of their interaction.

Conclusions

The mechanochemical synthesis of Fe-doped ATLS has been studied. The possibility of a partial substitution of Si in the apatite with dopant and the mechanism of the formation of ATLS in the course of MA are revealed to depend on the nature of the dopant parent compound. The data obtained indicate that, in the course of milling, apatite-type lanthanum silicates can be formed by the cluster-topotactic or dissociative mechanism. The cluster-topotactic mechanism is favored by the structural compatibility of La_2O_3, $La(OH)_3$, and apatite, the formation of the intermediate amorphous ferrosilicate in the case of $Fe(NO_3)_3/SiO_2$ as Fe-precursor, in turn, favoring the incorporation of Fe into the apatite at room temperature. The incorporation of the dopant into the apatite structure is partially or fully hampered through milling when FeO(OH) and α-Fe_2O_3 are used as reagents. The presence of appreciable amounts of H_2O in the reaction space due to the decomposition of the starting $Fe(HCOO)_3$ crystalline hydrate leads to strong hydration of ions, favoring the destruction of mixture component structures and resulting in the formation of apatite through a dissociative mechanism. Using powders prepared by MA allows dense pellets of Fe-doped apatites to be obtained at a lower temperature and with a shorter sintering time as compared with the conventional solid-state method.

Experimental Section

General: SiO_2 (REACHIM, 99.9%), La_2O_3 (VEKTON, 99.99%), and a number of different dopant precursors were used as parent compounds to synthesize ATLS. Fe_2O_3 (REACHIM, 99.5%), $Fe(HCOO)_3$ (REACHIM, 99.5%), FeO(OH) (REACHIM, 99.5%), and $Fe(NO_3)_3/SiO_2$ were used as Fe precursors for the preparation of Fe-doped samples. The latter precursor was prepared by wetness impregnation of SiO_2 by a water solution of iron nitrate, $Fe(NO_3)_3 \cdot 9H_2O$ (VEKTON, 99.9%) or from metallic ^{57}Fe dissolved in nitric acid (0.1 mol/L), followed by drying under a lamp. Before using, all parent compounds were characterized by XRD, IR spectroscopy, and thermal analysis to provide target sample stoichiometry and correct interpretation of data obtained.

For activation of stoichiometric mixtures, a planetary ball mill AGO-2 (steel dram volume 150 mL; steel balls diameter 8 mm) was used. For all samples discussed, the rate of the disc rotation and the ball-to-sample mass ratio were 1200 rpm (40 g) and ca. 30, respectively. Samples were activated for 1–15 or 1–30 min for a kinetic study and for 15 min for the estimation of the result of MA. To provide a correct synthesis with minor contamination from vessels and balls, a preliminary treatment of drams and balls was used. For this the activation of a portion of the corresponding mixture was performed before the synthesis, which results in covering the drum and ball surface by a layer of the mixture activated. Such procedure was earlier shown to essentially decrease the impurity amount ($<0.05 \pm 0.01$ wt.-%).[12,31] Unless specially stated, the products of MA were calcined at 900 and 1200 °C for 5 h. The samples after activation and the calcined ones were characterized by XRD and IR, UV/Vis electron, and Mössbauer spectroscopy.

Thermal analysis of the starting compounds was carried out with a Q-1500D or a NETZSCH STA 449 °C thermoanalyzer. XRD patterns were recorded with ARL′TRA θ-θ diffractometers with Si (Li) detector by using Cu-K_α radiation. IR spectra were recorded at room temperature with a Shimadzu FTIR-8300 spectrometer by using KBr pellets. UV/Vis spectra were collected at room temperature with a Shimadzu UV-2501 PC spectrometer equipped with a diffuse reflectance accessory (ISR-240 A) by using a $BaSO_4$ reflectance standard. Room-temperature Mössbauer spectra were acquired for samples doped with ^{57}Fe by using a NF-640 spectrometer and ^{57}Co (Pd) as a source.

Acknowledgments

This work is supported by the European Commission 6th Framework Program within the Novel Materials for Silicate-Based Fuel Cell Project (MATSILC).

[1] a) S. Nakayama, H. Aono, Y. Sadaoka, *Chem. Lett.* **1995**, *24*, 431–442; b) S. Nakayama, T. Kageyama, H. Aono, Y. Sadaoka, *J. Mater. Chem.* **1995**, *5*, 1801–1805; c) S. Nakayama, M. Sakamoto, *J. Eur. Ceram. Soc.* **1998**, *18*, 1413–1418.
[2] a) J. E. H. Sansom, D. Richings, P. R. Slater, *Solid State Ionics* **2001**, *139*, 205–210; b) J. R. Tolchard, M. S. Islam, P. R. Slater, *J. Mater. Chem.* **2003**, *13*, 1956–1961.
[3] a) L. Leon-Reina, E. R. Losilla, M. Martinez-Lara, S. Bruque, M. A. G. Aranda, *J. Mater. Chem.* **2004**, *14*, 1142–1149; b) L. Leon-Reina, E. R. Losilla, M. Martinez-Lara, S. Bruque, A. Llobet, D. V. Sheptyakovc, M. A. G. Aranda, *J. Mater. Chem.* **2005**, *15*, 2489–2498; c) L. Leon-Reina, J. M. Porras-Vazquez, E. R. Losilla, M. A. G. Aranda, *Solid State Ionics* **2006**, *177*, 1307–1315.
[4] J. R. Tolchard, P. R. Slater, *J. Phys. Chem. Solids* **2008**, *69*, 2433–2439.
[5] A. Najib, J. E. H. Sansom, J. R. Tolchard, P. R. Slater, M. S. Islam, *Dalton Trans.* **2004**, 3106–3109.
[6] a) J. E. H. Sansom, E. Kendrick, J. R. Tolchard, M. S. Islam, P. R. Slater, *J. Solid State Electrochem.* **2006**, *10*, 562–568; b) E. Kendrick, M. S. Islam, P. R. Slater, *J. Mater. Chem.* **2007**, *17*, 3104–3111.
[7] A. L. Shaula, V. V. Kharton, F. M. B. Marques, *J. Solid State Chem.* **2005**, *178*, 2050–2061.
[8] R. Riedel, I-W. Chen (Eds.), *Ceramics Science and Technology Vol. 1: Structures*, Wiley-VCH, Weinheim, **2008**, pp. 3–38.
[9] a) S. Celerier, C. Laberty, F. Ansart, P. Lenormand, P. Stevens, *Ceram. Int.* **2006**, *32*, 271–276; b) S. Celerier, C. Laberty-Robert, F. Ansart, C. Calmet, P. Stevens, *J. Eur. Ceram. Soc.* **2005**, *25*, 2665–2668.
[10] S. Tao, J. T. S. Irvine, *Mater. Res. Bull.* **2001**, *36*, 1245–1258.
[11] a) A. F. Fuentes, E. Rodriguez-Reyna, L. G. Martines-Gonzalez, M. Maczka, J. Hanuza, U. Amador, *Solid State Ionics* **2006**, *177*, 1869–1873; b) E. Rodriguez-Reyna, A. F. Fuentes, M. Maczka, J. Hanuza, K. Boulahya, U. Amador, *J. Solid State Chem.* **2006**, *179*, 522–531; c) A. F. Fuentes, L. G. Martines-Gonzalez, K. J. Moreno, E. Rodriguez-Reyna, U. Amador, *Mater. Res. Soc., Symp. Proc. Vol.* 972, 0972-AA09–05; d) L. G. Martines-Gonzalez, E. Rodriguez-Reyna, K. J. Moreno, J. I. Escalante-Garcia, A. F. Fuentes, *J. Alloys Compd.* **2009**, *476*, 710–714.
[12] T. Kharlamova, S. Pavlova, V. Sadykov, M. Chaikina, T. Krieger, O. Lapina, D. Khabibulin, A. Ishchenko, V. Zaikovskii, C. Argirusis, J. Frade, *Eur. J. Inorg. Chem.* **2008**, *6*, 939–947.
[13] V. V. Zyryanov, *Advanc. Chem.* **2008**, *77*, 1–31.
[14] M. V. Chaikina, *Mechanochemistry of Natural and Synthetic Apatites* (Ed.: E. G. Avvakumov), Publishing House of SB RAS, Branch GEO, Novosibirsk, **2002**, p. 223.
[15] G. Tzvetkov, N. Minkova, *Mater. Lett.* **1999**, *39*, 354–358.
[16] I. I. Plusnina, *Infrared Spectra of Silicates*, Moscow University, **1967**, p. 190.
[17] O. V. Krylov, *Heterogeneous Catalysis*, M. PTC "Academkniga", **2004**, pp. 244–245.
[18] S. Bordiga, R. Buzzoni, F. Geobaldo, C. Lamberti, E. Giamello, A. Zecchina, G. Leofanti, G. Petrini, G. Tozzola, G. Vlaic, *J. Catal.* **1996**, *158*, 486–501.
[19] S. E. Malichin, V. F. Anufrienko, E. Jh. M. Hansen, E. V. Kusnetsova, T. V. Larina, J. M. Jidomirov, *J. Struct. Chem.* **2007**, *48*, 914–920.
[20] A. B. P. Lever, *Inorganic Electronic Spectroscopy*, Elsevier, Amsterdam, **1968**, p. 420.
[21] J. McFarlane, S. Barth, M. Swaffer, J. E. H. Sansom, P. R. Slater, *Ionics* **2002**, *8*, 149–154.
[22] A. L. Shaula, V. V. Kharton, J. C. Waerenborgh, D. P. Rojas, F. M. B. Marques, *J. Eur. Ceram. Soc.* **2005**, *25*, 2583–2586.
[23] T. Kharlamova, S. Pavlova, V. Sadykov, O. Lapina, D. Khabibulin, T. Krieger, V. Zaikovskii, A. Ishchenko, A. Salanov, V. Muzykantov, N. Mezentseva, M. Chaikina, N. Uvarov, J. Frade, C. Argirusis, *Solid State Ionics* **2008**, *179*, 1018–1023.
[24] P. Ratnasamy, R. Kumar, *Catal. Today* **1991**, *9*, 329–416.
[25] A. A. Yaremchenko, A. L. Shaula, V. V. Kharton, J. C. Waerenborgh, D. P. Rojas, M. V. Patrakeev, F. M. B. Marques, *Solid State Ionics* **2004**, *171*, 51–59.
[26] T. Kharlamova, S. Pavlova, V. Sadykov, T. Krieger, L. Batuev, V. Muzykantov, N. Uvarov, C. Argirusis, *Solid State Ionics* **2009**, *180*, 796–799.
[27] E. G. Avvakumov, *Chem. Sustainable Dev.* **1994**, *2*, 485–498.
[28] P. Y. Butyagin, *Russ. Chem. Rev.* **1984**, *53*, 1025–1038.
[29] L. S. D. Glasser, F. P. Glasser, H. F. W. Taylor, *Q. Rev., Chem. Soc.* **1962**, *16*, 343–360.
[30] I. Bonev, *Acta Crystallogr., Sect. A* **1972**, *28*, 508–512.
[31] T. Kharlamova, S. Pavlova, V. Sadykov, O. Lapina, D. Khabibulin, T. Krieger, V. Zaikovskii, A. Ishchenko, M. Chaikina, C. Argirusis, *J. Chem. Eng. Jpn.* **2007**, *40*, 1187–1191.

Received: September 2, 2009
Published Online: December 17, 2009

